Remotely sensing an object's rotational orientation using the orbital angular momentum of light

(Invited Paper)

Giovanni Milione[1,*], Ting Wang[1], Jing Han (韩 静)[2], and Lianfa Bai (柏连发)[2]

[1]*Optical Networking and Sensing Department, NEC Laboratories America, Inc., Princeton, NJ 08540, USA*
[2]*School of Electronic Engineering and Optoelectronic Technology, Nanjing University of Science and Technology, Nanjing 210094, China*
**Corresponding author: gmilione@nec-labs.com*

Received January 11, 2017; accepted February 13, 2017; posted online February 28, 2017

Remotely sensing an object with light is essential for burgeoning technologies, such as autonomous vehicles. Here, an object's rotational orientation is remotely sensed using light's orbital angular momentum. An object is illuminated by and partially obstructs a Gaussian light beam. Using an SLM, the phase differences between the partially obstructed Gaussian light beam's constituent OAM modes are measured analogous to Stokes polarimetry. It is shown that the phase differences are directly proportional to the object's rotational orientation. Comparison to the use of a pixelated camera and implementation in the millimeter wave regime are discussed.

OCIS codes: 280.4788, 280.3420, 260.6042, 080.4865, 140.3295.
doi: 10.3788/COL201715.030012.

Remotely sensing an object with light comprises illuminating the object with light, and then, measuring the transmitted, reflected, or scattered light. The facet of the object that is sensed depends on the facet of light that is measured. For example, an object's chemical composition can be sensed by measuring light's wavelength (*e.g.*, hyperspectral imaging)[1].

Remotely sensing an object with light is essential for burgeoning technologies, such as autonomous vehicles. Of importance is remotely sensing an object's rotational orientation, which enables navigation functionalities, such as determining the pose. Conventional methods to do this include capturing an image of the object using a pixelated camera[2].

There is interest in a facet of light referred to as orbital angular momentum (OAM). A light beam that propagates in the z direction and has a phase of $\exp(i\ell\phi)$ is referred to as an OAM mode, where (r, ϕ, z) are cylindrical coordinates. An OAM mode has an OAM of $\ell\hbar$ per photon ($\ell = 0, \pm1, \pm2, ...$) where $\hbar$ is Planck's reduced constant[3]. OAM modes make up a complete orthogonal set. An arbitrary light beam's amplitude is a superposition of OAM modes given by[4]

$$u(r,\phi) = \sum_{\ell} c_{\ell}(r)\exp(i\ell\phi), \tag{1}$$

where $c_{\ell}(r)$ are complex coefficients, and the summation is over all ℓ. The OAM modes' powers and phases are given by

$$P_{\ell} = \int_0^{\infty} r\mathrm{d}r|c_{\ell}|^2, \tag{2}$$

$$\theta_{\ell} = \arg\left(\int_0^{\infty} r\mathrm{d}r c_{\ell}(r)\right), \tag{3}$$

where

$$c_{\ell}(r) = \int_0^{\infty} r\mathrm{d}r \int_0^{2\pi} \mathrm{d}\phi u(r,\phi)\exp(-i\ell\phi). \tag{4}$$

The powers of the OAM modes that make up a light beam are referred to as its spiral spectrum.

OAM modes and other modes are used for optical communication[5–13]. Like other facets of light, OAM modes can be used for remote sensing. By illuminating an object with light, and then measuring the transmitted, reflected, or scattered light's spiral spectrum [Eq. (2)], an object's structure, rotational velocity, and lateral motion were remotely sensed[14–21]. However, in these works, the phases of a light beam's constituent OAM modes [Eq. (3)] are not measured and an object's rotational orientation is not remotely sensed.

The phase differences between a light beam's constituent OAM modes are proportional to the light beam's rotational orientation[22–25]. This is analogous to the phase differences between a light beam's right and left circular polarization states being proportional to its state of the polarization's rotational orientation. As such, it may be possible to remotely sense an object's rotational orientation by measuring the phase differences between a light beam's constituent OAM modes.

Here, an object's rotational orientation is remotely sensed using light's OAM. An object is illuminated by and partially obstructs a Gaussian light beam. Using a spatial light modulator (SLM), the phase differences between the partially obstructed Gaussian light beam's constituent

OAM modes are measured analogous to Stokes polarimetry. It is shown that the phase differences are directly proportional to the object's rotational orientation. Comparison to the use of a pixelated camera and implementation in the millimeter wave regime are discussed.

Consider a Gaussian light beam that propagates in the z direction. It's amplitude is $u(r,\phi) \propto \exp(-r^2/w_o^2)$. w_o is the waist size. For simplicity, the divergence is neglected. The Gaussian light beam is partially obstructed by an object in the x–y plane (r–ϕ-plane). The object is larger than w_o. (x, y) are Cartesian coordinates $(r^2 = x^2 + y^2; \phi = \tan^{-1}(y/x))$. Because the Gaussian light beam is partially obstructed, it has a rotational orientation in the x–y plane. It is defined by the angle ϕ_o. ϕ_o is the angle the object's edge makes with respect to the x axis. Figures 1(a1), 1(b1), and 1(c1) schematically show three orientations, $\phi_o = 0, \pi/4$, and $\pi/2$, respectively (half of the Gaussian light beam is obstructed). For each orientation, the partially obstructed Gaussian light beam's spiral spectrum and the phase differences between its constituent OAM modes were theoretically calculated using Eqs. (1)–(4). The results are shown in Figs. 1(a2), 1(b2), and 1(c2), respectively. Note that the OAM spectra

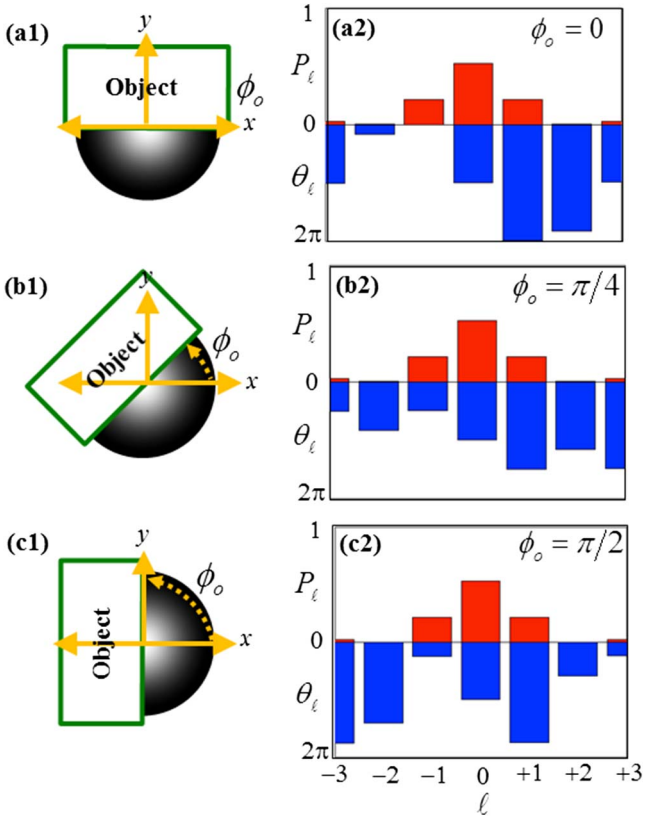

Fig. 1. Schematics of a Gaussian light beam that is partially obstructed by an object that has a rotational orientation (ϕ_o) and theoretically calculated spiral spectra and phase differences of the partially obstructed Gaussian light beam's constituent OAM modes as described in the text. The spiral spectra are normalized with respect to the sum of the powers of OAM modes from $\ell = -10$ to $\ell = +10$. The phase differences are relative to the phase of the $\ell = 0$ OAM mode.

agree with previous work[26]. As can be seen, the spiral spectra do not depend on ϕ_o. However, the phase differences between the OAM modes do. Therefore, when an object is illuminated by and partially obstructs a Gaussian light beam the objects' rotational orientation may be remotely sensed by measuring the phase differences between the partially obstructed Gaussian light beam's constituent OAM modes.

The experimental setup is shown in Fig. 2. As shown in Fig. 2(a), an $f1 = 8$ mm focal length lens (L1) was used to expand and collimate a Gaussian light beam ($\lambda = 1550$ nm) from a single mode optical fiber (SMF1) ($w_o \sim 1$ mm). The Gaussian light beam illuminated and was partially obstructed by a razor blade (R). R served as the object. R was much larger than w_o. R's edge was oriented perpendicular to the lab table. The edge's position with respect to the Gaussian light beam's center was controlled using a translation stage. A $4f$ imaging system comprised of two $f2, f3 = 20$ cm focal length lenses (L2, L3) imaged the partially obstructed Gaussian light beam onto the display of a reflective phase-only (0–2π) liquid crystal on silicon SLM. The SLM displayed a computer generated hologram (CGH). As shown in Fig. 2(b), the partially obstructed Gaussian light beam back-reflected off of the SLM display. Using the $4f$ imaging system (L2,L3) and a non-polarizing beam splitter (BS, which is not shown), the back-reflected partially obstructed Gaussian light beam was imaged onto the back focal plane of another $f4 = 8$ mm focal length lens (L4). Finally, using a non-polarizing BS, which is not shown. Finally, the partially obstructed Gaussian light beam was focused into another single mode optical fiber using L4 (SMF2).

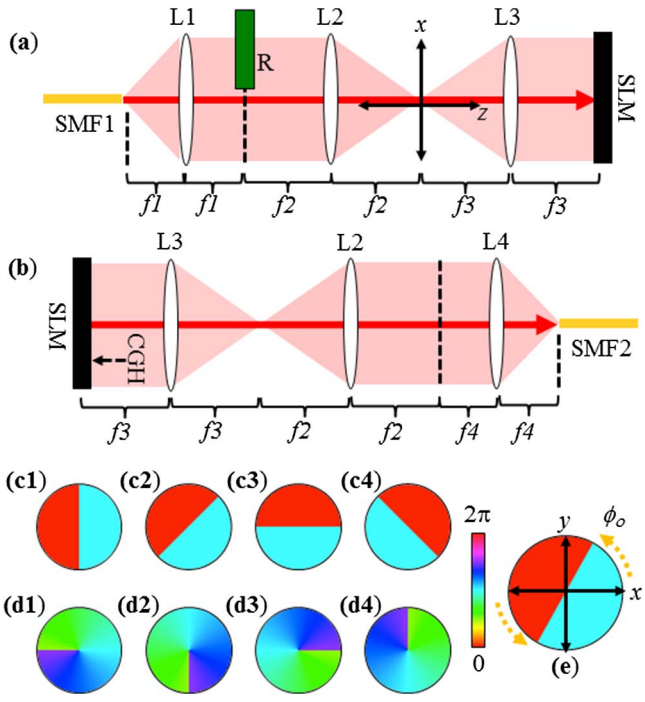

Fig. 2. Experimental setup as described in the text.

The phase differences between the partially obstructed Gaussian light beam's constituent OAM modes were measured analogous to Stokes polarimetry. In Stokes polarimetry, the phase difference between a light beam's constituent right and left circular polarization states is measured by measuring the light beam's power after it propagates through a linear polarizer whose transmission axis is oriented at 0°, 45°, 90°, and 135° with respect to the lab table. The measured power is given by I_0, I_{45}, I_{90}, and I_{135}, respectively. The phase difference between the right and left circular polarization is given by[27]

$$\theta = \tan^{-1}\left(\frac{I_0 - I_{90}}{I_{45} - I_{135}}\right). \tag{5}$$

The phase difference between two OAM modes can be measured analogously. For two OAM modes, I_0, I_{45}, I_{90}, and I_{135} can be holographically measured by displaying corresponding CGHs on the SLM, and then measuring the power after SMF2[28,29]. Effectively, the CGHs are plots of the phases of the superpositions of the two OAM modes when they have an appropriate phase difference. I_0, I_{45}, I_{90}, and I_{135} correspond to the phase differences of 0, $\pi/2$, π, and $3\pi/2$, respectively. CGHs corresponding to I_0, I_{45}, I_{90}, and I_{135} that are used to measure the phase difference between the $\ell = -1$ and $\ell = +1$ OAM modes are shown in Figs. 2(c1), 2(c2), 2(c3), and 2(c4), respectively. CGHs corresponding to I_0, I_{45}, I_{90}, and I_{135} that are used to measure the phase difference between the $\ell = 0$ and $\ell = +1$ OAM modes are shown in Figs. 2(d1), 2(d2), 2(d3), and 2(d4), respectively.

As can be seen in Fig. 1, the spiral spectra of the partially obstructed Gaussian light beam comprises power predominantly from the $\ell = -1$, $\ell = 0$, and $\ell = +1$ OAM modes. Therefore, the phase differences between the $\ell = -1$ and $\ell = +1$ OAM modes and the $\ell = 0$ and $\ell = +1$ OAM modes were measured.

Instead of physically rotating R, R's rotational orientation (ϕ_o) was emulated by digitally rotating the CGHs, as shown in Fig. 2(e). Rotating the CGHs and keeping R fixed is equivalent to rotating R and keeping the CGHs fixed. Note that while not shown here, the CGHs were given a linear grating, so that SMF2 was aligned to a resulting first diffraction order in the L4 focal plane.

Using the experimental setup described above, the phase differences between the $\ell = -1$ and $\ell = +1$ OAM modes of the partially obstructed Gaussian light beam were measured as a function of ϕ_o. CGHs corresponding to I_0, I_{45}, I_{90}, and I_{135}, as shown in Figs. 2(c1), 2(c2), 2(c3), and 2(c4), were displayed on the SLM one at a time. The power (intensity) after SMF2 was measured when each CGH was rotated in steps of $2\pi/100$ from $\phi_o = 0$ to $\phi_o = 2\pi$. The results and theoretical calculations that are calculated using Eqs. (1)–(4) are shown in Fig. 3(a). Using these results, the phase differences between the $\ell = -1$ and $\ell = +1$ OAM modes were calculated using Eq. (5) (θ). The results and theoretical calculations that were calculated using Eqs. (1)–(4) are

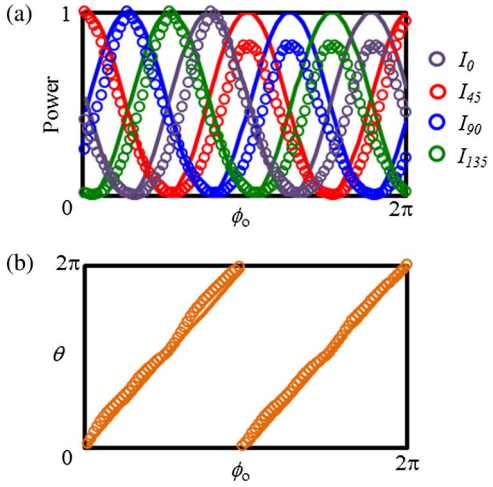

Fig. 3. Measured phase differences (θ) between the $\ell = -1$ and $\ell = +1$ OAM modes of the partially obstructed Gaussian light beam as a function of the rotation angle (ϕ_o) as described in the text. Circles represent measured values. Solid lines represent theoretically calculated values. Note that the error bars are smaller than the markers.

shown in Fig. 3(b). As can be seen, ϕ_o is directly proportional to θ. However, note that the results repeat at $\phi_o = \pi$. As a result, when measuring the phase differences between the $\ell = -1$ and $\ell = +1$ OAM modes, the object's rotational orientation can be remotely sensed from $\phi_o = 0$ to $\phi_o = \pi$.

Using the experimental setup described above, the phase differences between the $\ell = 0$ and $\ell = +1$ OAM modes of the partially obstructed Gaussian light beam were measured as a function of ϕ_o. CGHs corresponding to I_0, I_{45}, I_{90}, and I_{135}, as shown in Fig. 2(d1), 2(d2), 2(d3), and 2(d4), were displayed on the SLM one at a

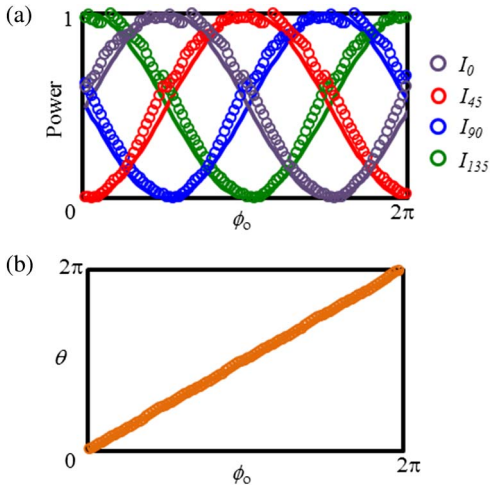

Fig. 4. Measured phase differences (θ) between the $\ell = 0$ and $\ell = +1$ OAM modes of the partially obstructed Gaussian light beam as a function of the rotation angle (ϕ_o) as described in the text. Circles represent measured values. Solid lines represent theoretically calculated values. Note that the error bars are smaller than the markers.

time. The power (intensity) after SMF2 was measured when each CGH was rotated in steps of $2\pi/100$ from $\phi_o = 0$ to $\phi_o = 2\pi$. The results and theoretical calculations that were calculated using Eqs. (1)–(4) are shown in Fig. 4(a). Using these results, the phase differences between the $\ell = 0$ and $\ell = +1$ OAM modes were calculated using Eq. (5) (θ). The results and theoretical calculations that were calculated using Eqs. (1)–(4) are shown in Fig. 4(b). As can be seen, ϕ_o is directly proportional to θ. In contrast to Fig. 3, the results do not repeat at $\phi_o = \pi$. As a result, when measuring the phase differences between the $\ell = 0$ and $\ell = +1$ OAM modes, the object's rotational orientation can be remotely sensed from $\phi_o = 0$ to $\phi_o = 2\pi$.

Using the experimental setup described above, the phase differences between the $\ell = -1$ and $\ell = +1$ OAM modes of the partially obstructed Gaussian light beam were measured as a function of ϕ_o for three varying positions of R's edge with respect the light beam's center. R's position was controlled using a translation stage. R's position was made to be at the light beam's center, half a waist size ($w_o/2$) away from the light beam's center, and one waist size (w_o) away from the light beam's center, as schematically shown in Figs. 5(a1), 5(b1), and 5(c1), respectively. For each position, CGHs corresponding to I_0, I_{45}, I_{90}, and I_{135}, as shown in Figs. 2(d1), 2(d2), 2(d3), and 2(d4), were displayed on the SLM one at a time. The power (intensity) after SMF2 was measured when each CGH was rotated in steps of $2\pi/100$ from $\phi_o = 0$ to $\phi_o = 2\pi$. Using these results, the phase differences between the $\ell = -1$ and $\ell = +1$ OAM modes were calculated using Eq. (5) (θ). For each position, the results and theoretical calculations, which were calculated using Eqs. (1)–(4), are shown in Figs. 5(b1), 5(b2), and 5(b3), respectively. As can be seen, regardless of the position of R's edge with respect the light beam's center, the phase differences between the $\ell = -1$ and $\ell = +1$ OAM modes can be measured.

In conclusion, an object's rotational orientation is remotely sensed using light's OAM. An object is illuminated by and partially obstructed a Gaussian light beam. Using an SLM, the phase differences between the partially obstructed Gaussian light beam's constituent OAM modes are measured analogous to Stokes polarimetry. It is shown that the phase differences are directly proportional to the object's rotational orientation.

Remotely sensing an object with light is essential for burgeoning technologies, such as autonomous vehicles. Remotely sensing an object's rotational orientation enables navigation functionalities, such as determining the pose. Conventional methods to do this include capturing an image of the object using a pixelated camera[2]. Compared to using a pixelated camera, the method describe above may not be as practical. However, for autonomous vehicles, a millimeter wave radar is often used instead of or in addition to pixelated cameras. This method may be implemented in the millimeter wave regime. The measurement of OAM in the millimeter wave regime has been demonstrated[30–32].

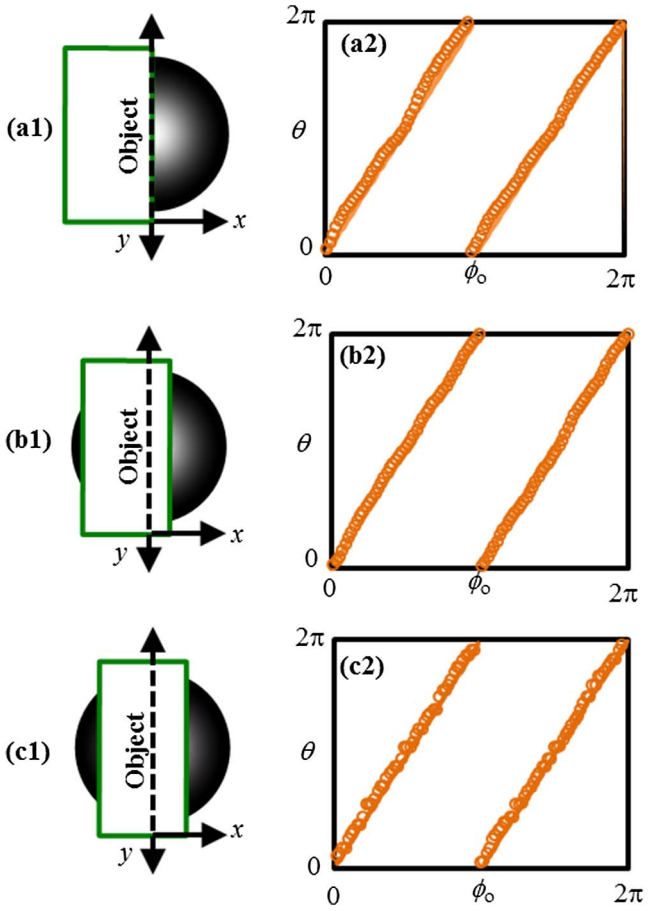

Fig. 5. Measured phase differences (θ) between the $\ell = -1$ and $\ell = +1$ OAM modes of the partially obstructed Gaussian light beam for three varying positions of R's edge with respect to the light beam's center as described in the text. Circles represent measured values. Solid lines represent theoretically calculated values. Note that the error bars are smaller than the markers.

Here, the phase differences between the $\ell = -1$ and $\ell = +1$ and the $\ell = 0$ and $\ell = +1$ OAM modes are measured. However, in principle, the phase differences between other OAM modes may be measured, e.g., $\ell = 0$ and $\ell = +2$ or $\ell = +1$ and $\ell = +2$ OAM modes. As shown above, when measuring the phase differences between the $\ell = -1$ and $\ell = +1$ OAM modes, the object's rotational orientation can be remotely sensed from $\phi_o = 0$ to $\phi_o = \pi$. However, when measuring the phase differences between the $\ell = 0$ and $\ell = +1$ OAM modes, the object's rotational orientation can be remotely sensed from $\phi_o = 0$ to $\phi_o = 2\pi$. This is due to the rotational symmetry of the OAM modes, which is illustrated via the CGHs in Fig. 2. This will be similar when measuring the phase differences between other OAM modes.

Also, here, the phase differences between the $\ell = -1$ and $\ell = +1$ and the $\ell = 0$ and $\ell = +1$ OAM modes are measured because the spiral spectra of the partially obstructed Gaussian light beam comprised power predominantly from the $\ell = -1$, $\ell = 0$, and $\ell = +1$ OAM

modes. However, if a different light beam were to illuminate the object, such as an $\ell = +2$ OAM mode or a superposition of the OAM modes, then the corresponding spiral spectra may comprise considerable power in other OAM modes whose phase differences could be measured.

A combination of using a different light beam to illuminate the object and measuring the phase differences between other OAM modes may be useful when remotely sensing more complex objects.

Additionally, it may be of interest to investigate comparable methods of remote sensing using other modes, such as vector beams[33–39].

References

1. J. B. Campbell and R. H. Wynne, *Introduction to Remote Sensing* (Guilford, 2011).
2. C. Urmson, J. Anhalt, D. Bagnell, C. Baker, R. Bittner, M. Clark, J. Dolan, D. Duggins, T. Galatali, C. Geyer, M. Gittleman, S. Harbaugh, M. Hebert, T. Howard, S. Kolski, A. Kelly, M. Likhachev, M. McNaughton, N. Miller, K. Peterson, B. Pilnick, R. Rajkumar, P. Rybski, B. Salesky, Y. Seo, S. Singh, J. Snider, A. Stentz, W. Whittaker, Z. Wolkowicki, J. Ziglar, H. Bae, T. Brown, D. Demitrish, B. Litkouhi, J. Nickolaou, V. Sadekar, W. Zhang, J. Struble, M. Taylor, M. Darms, and D. Ferguson, J. Field Rob. **25**, 425 (2008).
3. A. Yao and M. J. Padgett, Adv. Opt. Photon. **3**, 161 (2011).
4. G. Molina-Terriza, J. P. Torres, and L. Torner, Phys. Rev. Lett. **88**, 013601 (2002).
5. H. Huang, G. Milione, M. P. J. Lavery, G. Xie, Y. Ren, Y. Cao, N. Ahmed, T. A. Nguyen, D. A. Nolan, M.-J. Li, M. Tur, R. R. Afano, and A. E. Willner, Sci. Rep. **5**, 14931 (2015).
6. G. Milione, M. P. J. Lavery, H. Huang, Y. Ren, G. Xie, T. A. Nguyen, E. Karimi, L. Marrucci, D. A. Nolan, R. R. Alfano, and A. E. Willner, Opt. Lett. **40**, 1980 (2015).
7. G. Milione, T. A. Nguyen, J. Leach, D. A. Nolan, and R. R. Alfano, Opt. Lett. **40**, 4887 (2015).
8. E. Ip, G. Milione, M.-J. Li, N. Cvijetic, K. Kanonakis, J. Stone, G. Peng, X. Prieto, C. Montero, V. Moreno, and J. Linares, Opt. Express **23**, 17120 (2015).
9. G. Milione, E. Ip, M.-Jun Li, J. Stone, G. Peng, and T. Wang, Opt. Lett. **41**, 2755 (2016).
10. G. Milione, E. Ip, Y.-K. Huang, P. Ji, T. Wang, M.-J. Li, J. Stone, and G. Peng, in *Proc. 21st Opto-Electronics and Communications Conference* (OECC, 2016), paper PD2-1.
11. G. Milione, P. Ji, E. Ip, M. J. Li, J. Stone, and G. Peng, in *Optical Fiber Communication Conference* (OFC, 2014), paper W1F.2.
12. G. Milione, D. A. Nolan, and R. R. Alfano, J. Opt. Soc. Am. B **32**, 143 (2015).
13. R. R. Alfano, G. Milione, E. J. Galvez, and L. Shi, Nat. Photon. **10**, 286 (2016).
14. L. Torner, J. Torres, and S. Carrasco, Opt. Express **13**, 873 (2005).
15. G. Molina-Terriza, L. Rebane, J. P. Torres, L. Torner, and S. Carrasco, J. Eur. Opt. Soc. **2**, 07014 (2007).
16. L. Chen, J. Lei, and J. Romero, Light **3**, e153 (2014).
17. N. Uribe-Patarroyo, A. Fraine, D. S. Simon, O. Minaeva, and A. V. Sergienko, Phys. Rev. Lett. **110**, 043601 (2013).
18. A. Belmonte, C. Rosales-Guzman, and J. P. Torres, Optica **2**, 1002 (2015).
19. M. Seghilani, M. Myara, I. Sagnes, B. Chomet, R. Bendoula, and A. Garnache, Opt. Lett. **40**, 5778 (2015).
20. H. Zhou, D. Fu, J. Dong, P. Zhang, and X. Zhang, Opt. Express **24**, 10050 (2016).
21. N. Cvijetic, G. Milione, E. Ip, and T. Wang, Sci. Rep. **5**, 15422 (2015).
22. L. Allen and M. J. Padgett, J. Mod. Opt. **54**, 487 (2007).
23. M. J. Padgett, G. Whyte, J. Girkin, A. Wright, L. Allen, P. Ohberg, and S. M. Barnett, Opt. Lett. **31**, 2205 (2006).
24. S. Franke-Arnold, G. Gibson, R. W. Boyd, and M. J. Padgett, Science **333**, 65 (2011).
25. E. Wisniewski-Barker, G. M. Gibson, S. Franke-Arnold, R. W. Boyd, and M. J. Padgett, Opt. Express **22**, 11690 (2014).
26. G. Gibson, J. Courtial, M. J. Padgett, M. Vasnetsov, V. Pas'ko, S. M. Barnett, and S. Franke-Arnold, Opt. Express **12**, 5448 (2004).
27. A. Dudley, G. Milione, R. R. Alfano, and A. Forbes, Opt. Express **22**, 14031 (2014).
28. J. Leach, B. Jack, J. Romero, M. Ritsch-Marte, R. W. Boyd, A. K. Jha, S. M. Barnett, S. Franke-Arnold, and M. J. Padgett, Opt. Express **17**, 8287 (2009).
29. A. Forbes, A. Dudley, and M. McLaren, Adv. Opt. Photon. **8**, 200 (2016).
30. Y. Yan, L. Li, G. Xie, C. Bao, P. Liao, H. Huang, Y. Ren, N. Ahmed, Z. Zhao, Z. Wang, N. Ashrafi, S. Ashrafi, S. Talwar, S. Sajuyigbe, M. Tur, A. F. Molisch, and A. E. Willner, Sci. Rep. **6**, 33482 (2016).
31. G. Xie, Z. Zhao, Y. Yan, L. Li, Y. Ren, N. Ahmed, Y. Cao, A. J. Willner, C. Bao, Z. Wang, C. Liu, M. Ziyadi, S. Talwar, S. Sajuyigbe, S. Ashrafi, M. Tur, A. F. Molisch, and A. E. Willner, Sci. Rep. **6**, 37078 (2016).
32. Y. Yan, G. Xie, M. P. J. Lavery, H. Huang, N. Ahmed, C. Bao, Y. Ren, Y. Cao, L. Li, Z. Zhao, A. F. Molisch, M. Tur, M. J. Padgett, and A. E. Willner, Nat. Commun. **5**, 4876 (2014).
33. G. Milione, H. I. Sztul, D. A. Nolan, and R. R. Alfano, Phys. Rev. Lett. **107**, 053601 (2011).
34. G. Milione, S. Evans, D. A. Nolan, and R. R. Alfano, Phys. Rev. Lett. **108**, 190401 (2012).
35. G. M. Philip, V. Kumar, G. Milione, and N. K. Viswanathan, Opt. Lett. **37**, 2667 (2012).
36. Y. S. Rumala, G. Milione, T. A. Nguyen, S. Pratavieira, Z. Hossain, D. A. Nolan, S. Slussarenko, E. Karimi, L. Marrucci, and R. R. Alfano, Opt. Lett. **38**, 5083 (2013).
37. G. Milione, A. Dudley, T. A. Nguyen, O. Chakraborty, E. Karimi, A. Forbes, and R. R. Alfano, J. Opt. **17**, 035617 (2015).
38. G. Milione, H. Sztul, D. Nolan, J. Kim, M. Etienne, J. McCarthy, J. Wang, and R. Alfano, in *CLEO: 2011-Laser Applications to Photonic Applications* (2011), paper CTuB2.
39. G. Milione, H. I. Sztul, D. A. Nolan, J. Kim, M. Etienne, J. McCarthy, J. Wang, and R. R. Alfano, Proc. SPIE **7950**, 79500K (2011).